THE JOURNAL OF PHYSICAL CHEMISTRY A

Article

pubs.acs.org/JPCA

Nuclear Spin Symmetry Conservation in $^1H_2{}^{16}O$ Investigated by Direct Absorption FTIR Spectroscopy of Water Vapor Cooled Down in Supersonic Expansion

Robert Georges,[*,†] Xavier Michaut,[‡] Audrey Moudens,[‡] Manuel Goubet,[¶] Olivier Pirali,[§,#] Pascale Soulard,[∥] Pierre Asselin,[∥] Thérèse Huet,[¶] Pascale Roy,[§] Martin Fournier,[†] and Andrey Vigasin[⊥]

[†]Institut de Physique de Rennes, UMR6251, CNRS-Université de Rennes 1, Campus de Beaulieu, 35042 Rennes, France

[‡]Laboratoire d'Etudes du Rayonnement et de la Matière en Astrophysique et Atmosphères, Sorbonne Universities, UPMC Univ. Paris 06, Université de Cergy-Pontoise, Observatoire de Paris, PSL Research University, CNRS, F-75252 Paris, France

[¶]Université Lille, CNRS, UMR8523-PhLAM - Physique des Lasers, Atomes et Molécules, F-59000 Lille, France

[§]AILES beamline, Synchrotron SOLEIL, L'Orme des Merisiers, Saint Aubin BP 48, F-91192 Gif-sur-Yvette Cedex, France

[#]Institut des Sciences Moléculaires d'Orsay (ISMO), UMR 8214 CNRS, Univ. Paris-Sud, Université Paris-Saclay, F-91405 Orsay, France

[∥]Sorbonne Universités, UPMC Univ Paris 06, CNRS, UMR 8233, MONARIS, F-75005 Paris, France

[⊥]Obukhov Institute of Atmospheric Physics, Russian Academy of Sciences, 3 Pyzhevsky per, 119017 Moscow, Russia

ABSTRACT: We report the results of an experimental study related to the relaxation of the nuclear spin isomers of the water molecule in a supersonic expansion. Rovibrational lines of both *ortho* and *para* spin isomers were recorded in the spectral range of H_2O stretching vibrations at around 3700 cm^{-1} using FTIR direct absorption. Water vapor seeded in argon, helium, or oxygen or in a mixture of oxygen and argon was expanded into vacuum through a slit nozzle. The water vapor partial pressure in the mixture varied over a wide range from 1.5 to 102.7 hPa, corresponding to a water molar fraction varying between 0.2 and 6.5%. Depending on expansion conditions, the effect of water vapor clustering was clearly seen in some of our measured spectra. The Boltzmann plot of the line intensities allowed the H_2O rotational temperatures in the isentropic core and in the lateral shear layer probed zones of the planar expansion to be determined. The study of the *OPR*, i.e., the ratio of the *ortho* to *para* absorption line intensities as a function of T_{rot}, did not reveal any signs of the *OPR* being relaxed to the sample temperature. In contrast, the *OPR* was always conserved according to the stagnation reservoir equilibrium temperature. The conservation of the *OPR* was found irrespective of whether water molecule clustering was pronounced or not. Also, no effect of the paramagnetic oxygen admixture enhancing *OPR* relaxation was observed.

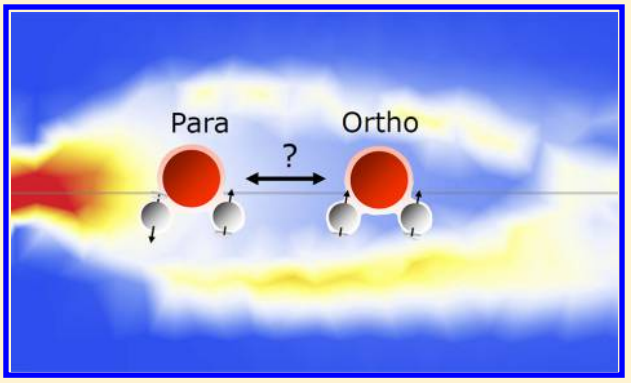

INTRODUCTION

Water is an asymmetric top molecule, and its rovibrational levels are conventionally labeled by $J_{K_aK_c}$, where J is the total rotational angular momentum quantum number and K_a and K_c are quantum numbers of the components of the total angular momentum on the principal axes a and c, respectively. These levels are assigned in the ground vibrational state to either *para* or *ortho* species for even or odd $K_a + K_c$, respectively. The notations are inverted in the antisymmetric vibrational stretch ν_3 state.

The two hydrogen nuclei in a water molecule have either parallel or antiparallel spins. Similar to the hydrogen molecule, the conversion between these two forms is strictly forbidden in an isolated water molecule and strongly improbable in the gas phase.[1] Water vapor can therefore be thought to be a mixture of two stable spin isomer forms: *ortho* and *para*. *Para* isomers, which have a total nuclear spin statistical weight g_{NS} equal to unity ($g_{NS} = 2I + 1$, where I is the total nuclear spin: $I_{para} = 0$, $I_{ortho} = 1$) are dominant in $^1H_2{}^{16}O$ water vapor at very low temperatures because the water molecule ground state belongs to the *para* subsystem of rotational energy levels. In contrast, thermal population of many rotational levels at elevated temperatures causes *ortho* isomers to dominate in a mixture

Received: July 12, 2017
Revised: September 14, 2017
Published: September 15, 2017

DOI: 10.1021/acs.jpca.7b06858
J. Phys. Chem. A XXXX, XXX, XXX−XXX

because of the higher nuclear spin statistical weight of *ortho* states. The limiting high-temperature *ortho*-to-*para* ratio (*OPR* = 3) of the nuclear spin isomer abundances is already reached at temperatures in excess of ca. 50 K, and it remains constant at higher temperature, including, of course, room temperature. Some experimental studies (see, e.g., ref 2) carried out on the supersonic cooling of water vapor seeded in Ar relied on the assumption that *OPR* = 3 is preserved in the jet expansion.

An introduction to recent studies of nuclear spin isomer conversion in water vapor can be found in the paper from Manca Tanner et al.[3] Much attention has been paid in the past few years (see, e.g., refs 5−9) to the spectroscopic investigation of whether the normal *OPR* can be significantly distorted at near room temperature following multiple adsorption and desorption of water molecules onto the surface of various porous media such as adsorbent charcoal or polymer sorbents. Following initial observations dating back almost 30 years,[4] there were more recent claims[5] that an increase of *OPR* up to 10 instead of 3 at near room temperature can be reached using a type of frontal gas chromatograph column. Moreover, it was claimed in ref 5 that the nonequilibrium *OPR* ratio can be conserved over a long period (months) when a spin isomer-enriched sample is frozen. Once heated and released from the ice, the vapor is still in its nonequilibrium spin isomer state. These experimental findings were then subject to a contradictory evaluation. There were attempts to reproduce experiments reported in ref 5, which yielded either at least partially positive[6,7] or entirely negative[1,8] results. To summarize, it can be stated nowadays that at least the idea of very slow spin isomer conversion in the condensed phase has not met any independent confirmation and has to be ruled out. In contrast, it has been shown that *ortho*−*para* conversion in the condensed phase can occur on a time scale of between milliseconds[9] and hours.[10−13] In general, the results obtained in ref 5 were characterized, e.g., in ref 3, as having a "nonstandard interpretation". It was suggested in particular (see, e.g., refs 8 and 14) that microwave radiation-induced desorption might be responsible for the effect observed in refs 4 and 5 and that no *ortho*−*para* enrichment occurred at all. This suggestion seems, however, unlikely because the experiments with a diode laser spectrometer[7] apparently have confirmed the phenomenon of *ortho*−*para* enrichment detected previously in ref 5 with the use of a backward wave oscillator (BWO).

The results reported in ref 3 showed a rapid change in the spin isomer state in a supersonic expansion of $^{1}H_{2}{}^{16}O$ water vapor seeded in argon at a relatively high water molar fraction. Whereas at a low water vapor molar fraction ($0.35 < x < 0.9\%$) in a mixture with the carrier gas the nuclear spin symmetry was conserved, at higher water molar fractions ($0.9 < x < 1.6\%$) the *OPR* was seen to be completely relaxed, i.e., the measured *OPR* responded to a low rotational temperature in expansion. This fast relaxation cannot be explained by intramolecular processes in an individual water molecule and was thus interpreted as a result of water cluster formation, which is able presumably to significantly facilitate nuclear spin conversion (NSC). The rapid transition from nuclear spin symmetry conservation to complete nuclear spin relaxation regimes within the narrow range of water mole fractions that was observed in ref 3 has not found a clear explanation up to now. An attempt to reproduce the results reported in ref 3 was undertaken recently in ref 15 using a diode laser spectroscopic examination of two water vapor *ortho* and *para* absorption lines in a H_2O seeded in Ar expansion. Virtually no signs of nuclear spin relaxation were observed irrespective of whether the clustering in an expansion was definitely present or not. No correlation between clustering in the expansion and nuclear-spin isomerization was thus observed.

The idea of water clusters promoting the nuclear spin relaxation process that was put forward in ref 3 has much in common with an assumption made initially in ref 16, where preferred clustering of heavy D_2O water molecules from their ground *ortho* state was first suggested. In their thorough recent study, Vilesov et al.[11] assumed to have formed small water clusters predominantly made up of *para*-H_2O isomers using water embedded in an Ar matrix at low temperature. By waiting for 1400 min for the complete NSC of water molecules in the Ar matrix at 4 K, they produced nearly 100% *para* molecules in solid Ar because the mostly populated energetic level at the considered temperature is the lowest rotational energy level of the *para* state (i.e., the $J_{K_aK_c} = 0_{00}$ state in the vibrational ground state). A fast warming up to 50 K of the matrix resulted in rapid evaporation of Ar atoms, leaving behind water clusters on the cold substrate. The sublimation of such ice showed that the *OPR* of the molecules released into the gas phase was equilibrated at the high temperature limit. If we assume that the ice prior to sublimation was a pure *para*-ice, the lifetime of *para*-H_2O in ice must be less than ∼30 min, a value that should be compared to a lifetime of a month, claimed in ref 5. The nuclear spin relaxation time in the gas-phase water dimer was estimated in ref 11 to exceed 3 ms. According to ref 11, rapid nuclear spin relaxation of the water dimer embedded in an Ar matrix is likely to occur on the time scale of a few minutes. All of these observations are invaluable for understanding the nature and the rate of NSC in various media including astrophysical environments. In the paragraphs below, we shall address the above estimates while discussing the results of our experiments.

The present paper aims at further investigation of the water molecule nuclear spin symmetry conservation and relaxation in a supersonic expansion of $^{1}H_{2}{}^{16}O$ water vapor seeded in argon, helium, or oxygen as carrier gases. Mid-infrared (MIR) spectra were recorded using the Jet-AILES apparatus[17] at the SOLEIL synchrotron facility.

The use of a supersonic jet cross-probed by a FTIR spectrometer has both advantages and disadvantages for the study of relaxation processes. On one hand, rapid adiabatic cooling of the core part of the jet gives rise to a significant thermal nonequilibrium, which can easily be observed in the high-resolution absorption spectra. Low values of the isentropic core rotational temperature result in a limited set of rotational levels being populated, and consequently, only a small number of rotational lines can be seen in the spectrum. Also, the formation of dimers and larger clusters in the cold part of a jet is clearly seen in the expansion of water vapor seeded in Ar, as was evidenced, e.g., in refs 18−20. The spectral shifts of the small cluster stretching bands were monitored in refs 18−20 as a function of successive solvation of pure water clusters by argon atoms. On the other hand, only fast relaxation processes can be studied in such an experimental geometry where the supersonic jet expanding from the slit reaches and crosses the IR beam in a few microseconds.

The effect of lateral shock waves and viscous shear layers was taken into account. This effect leads to multitemperature gas samples being probed at the same time. Thorough separation of spectral signatures into low-temperature and high-temperature

DOI: 10.1021/acs.jpca.7b06858
J. Phys. Chem. A XXXX, XXX, XXX−XXX

ones was made by means of a Boltzmann plot for the measured absorption line intensities, as described below. The use of a movable Pitot probe was used to characterize the supersonic expansion, which was then used for FTIR spectroscopic observations. Despite the presence of the small water cluster signatures in our obtained spectra, no transition to a nuclear spin relaxation regime was observed: the *OPR* derived from the spectra was conserved on a level characteristic of equilibrium conditions in the stagnation reservoir, that is, the *OPR* was always equal to 3 irrespective of the extremely low rotational temperature. In addition, no change in *OPR* was observed when the argon carrier gas was replaced by oxygen. The latter is known to enhance nuclear spin relaxation because of its associated magnetic moment.[10,21,22] On the basis of the results obtained, we are in a position to dismiss the hypothesis of a water clustering effect on nuclear spin relaxation and to question the origin of the nuclear spin relaxation reported previously for a similar experiment.[3]

EXPERIMENTAL SETUP AND RECORDING OF THE SPECTRA

Jet-AILES Apparatus. The Jet-AILES apparatus was used to record the MIR spectrum of water vapor cooled down to a rotational temperature between 10 and 42 K in a supersonic expansion. This experimental setup has already been described in detail in other studies.[17] Briefly, a planar supersonic jet was formed by expanding water vapor admixed in various carrier gases (argon, helium, oxygen) from a high-pressure reservoir (2 bar maximum) to a low-pressure chamber through a slit nozzle (60 mm × 36 μm or 60 mm × 18 μm).

This chamber was evacuated by two Roots pumps (Edwards EH 500 and 2600) backed by a primary pump (Edwards GV80 Drystar), delivering an effective pumping speed of 1800 m^3/h. The gas flow was probed with the modulated infrared (IR) light beam issuing from the rear parallel exit of the high-resolution interferometer (Bruker IFS 125HR) equipping the AILES beamline. The IR beam was focused into the gas expansion using a first set of gold-coated mirrors with a magnification factor of 1.14. After its absorption by the cold expansion, the IR beam was collected and focused by a second set of mirrors onto a liquid-nitrogen-cooled InSb detector connected to the interferometer. A combination of a CaF_2 beamsplitter and a tungsten lamp was chosen to investigate the OH stretching region located at around 3700 cm^{-1}.

The spectra were recorded within the spectral range between 3400 and 3900 cm^{-1} where strong absorption by water vapor ν_1 and ν_3 stretching bands can be detected. In high-resolution spectra (Figure 1), the number of intense rotational lines varies significantly as a function of rotational temperature. Despite the significantly good signal-to-noise ratio achieved, the noise level in high-resolution spectra did not permit detection of the weak, broad, and virtually structureless absorption bands that belong to water clusters. To examine the evolution of cluster content under various expansion conditions, it was necessary to repeat the measurements at a much lower instrumental resolution (1 cm^{-1}). Figure 2 shows that cluster absorption does manifest itself in the region of free-OH vibrations as well as bonded-OH vibrations as broad unresolved features accumulating contributions from $(H_2O)_n$ and $(H_2O)_nAr_m$ clusters presumably containing up to dozens of molecules.[20]

Each experimental condition (see Table 1) was repeated twice: a first recording was performed at high resolution (0.002 cm^{-1}, Boxcar apodization, iris aperture: 0.8 mm) to determine

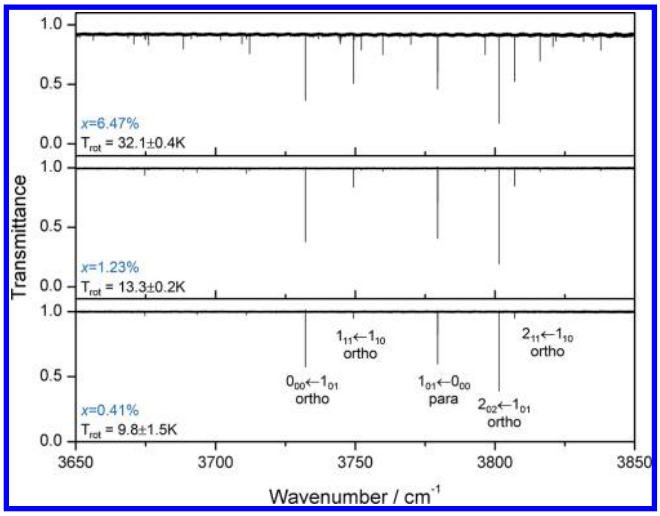

Figure 1. Selection of jet-cooled transmittance spectra recorded at 0.002 cm^{-1} resolution to avoid line saturation effects. Water clustering, driven by the partial pressure of water vapor present in the flow, is one of the means used to control the temperature of the flow (argon in these examples). Rotational temperature increases from the lower to the upper panel as the water molar fraction increases. In our study, relative intensities were calculated using four *ortho* transitions (given using the notation "band ν_3 ← ground state" by $2_{02} \leftarrow 1_{01}$; $0_{00} \leftarrow 1_{01}$; $1_{11} \leftarrow 1_{10}$; $2_{11} \leftarrow 1_{10}$) and one *para* transition ($1_{01} \leftarrow 0_{00}$).

the rotational temperature and the *OPR*, while a second one was performed at low resolution (1 cm^{-1}, triangle apodization, iris aperture: 0.8 mm) to track the presence of water clusters. The aperture setting was kept unchanged for high- and low-resolution recordings so that the dimensions of the IR beam through the flow remain unchanged (see Figure 3). Note that the spectrometer was maintained under high vacuum (1.2×10^{-4}–2.0×10^{-4} hPa) using a turbomolecular pump with active levitated magnetic bearings (Edwards model STP iX455), thus minimizing the contribution of atmospheric water to the absorption spectra.

The continuous water vapor production was controlled by a vapor generation CEM system (Controlled Evaporation and Mixing, Bronkhorst, model W-303A) consisting of a Coriolis liquid mass flow meter (mini Cori-Flow M12 Bronkhorst, ±0.2% of rate), a mass flow controller (model F-202AV Bronkhorst, ±0.5% Rd plus ±0.1% FS) for the carrier gas, and a temperature-controlled mixing and evaporation device. This system was used to vary the mass flow rate of water vapor between 2 and 100 g/h. The flow rate of the carrier gas was varied between 20 and 40 slm (1 standard liter per minute was measured at 0 °C and 1 atm). The water vapor molar fraction was varied between 0.21 and 6.91%. This interval was therefore larger than that corresponding to the former study reported in ref 3.

To avoid water condensation, the inlet gas lines were wrapped in heating wires and maintained at the appropriate temperature of 40 °C with a PID temperature controller. The gas reservoir and the nozzle were made from a block of tempered aluminum. The temperature of this element was regulated at 40 °C with two heating cartridges and a second PID temperature controller. The pressure of the gas reservoir was measured using a bakeable capacitance manometer (MKS Baratron 5000 Torr, model 615A) maintained at 100 °C to avoid water condensation in the gauge. The pressure of the

DOI: 10.1021/acs.jpca.7b06858
J. Phys. Chem. A XXXX, XXX, XXX−XXX

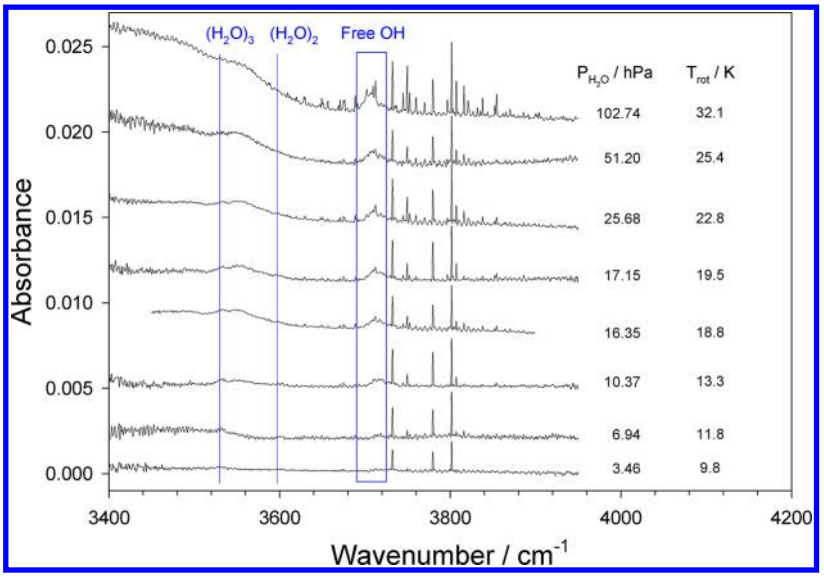

Figure 2. Series of low-resolution absorbances (offset for clarity) of water vapor cooled in argon (400 coadded scans at 1 cm^{-1} resolution). Water clustering is driven by the water vapor partial pressure (as indicated in the rightmost part of the figure) in the stagnation reservoir. In addition to the partially resolved water monomer lines, the signatures of both free OH (around 3710 cm^{-1}) and bound OH vibrations are observed.[20] The signatures of the water dimer and trimer can be seen at 3601 and 3533 cm^{-1}, respectively, for conditions leading to weak clustering. The broad absorption observed below 3600 cm^{-1} corresponds to much larger water clusters that form at enhanced water vapor partial pressure.

expansion chamber was measured with a 100 Torr full scale range Baratron (MKS model 626A).

Structure of the Supersonic Expansion. The supersonic expansion produced by one of the slit nozzles (60 mm × 18 μm) was carefully characterized with a Pitot probe. For this purpose, the slit nozzle was placed in a different vacuum chamber, at the University of Rennes (France), evacuated by a set of powerful mechanical pumps (15 000 m^3/h). A butterfly valve positioned between the vacuum chamber and the pumping unit was adjusted in order to match the pumping speed to that corresponding to the Jet-AILES apparatus (1800 m^3/h). The Pitot probe measured impact pressures from which the Mach number of the flow could be extracted. It is composed of a stainless steel capillary (outer diameter/inner diameter = 1.4/1.1 mm) connected to a capacitance manometer (MKS Baratron, 100 Torr) by a flexible tube. Its displacements in two perpendicular directions were controlled by two stepper motors with a precision better than 0.1 mm.

Figure 3 presents maps of various characteristics of the supersonic expansion of pure argon (20.1 slm), in a plane perpendicular to the long edge of the slit. The stagnation and residual pressures were 1072 and 0.68 hPa, respectively, thus very close to the conditions obtained with the Jet-AILES apparatus. Impact pressures measured by the Pitot probe are reported in this map, without any further treatment. It allows the diamond shock-cell pattern typical of an underexpanded free-jet expansion[18,19] to be visualized. A succession of three supersonic cells each about 20 mm long can be seen. The first cell (commonly known as the "zone of silence") is terminated by the intersection of the two lateral shocks 20 mm downstream from the nozzle exit. The lateral extension of this cell is about 8 mm at its largest width. The trace of the IR beam is sketched on the figure. The optical axis was set at about 5 mm from the nozzle exit. The inner circle of about 1 mm in diameter corresponds to the spot focus, positioned at the middle of the slit aperture, while the outer ellipse delimits the traces of the beam at the two edges of the slit. Part of the IR beam impinges on the lateral shocks and viscous shear layers, which are responsible for deceleration and compression of the flow. This effect leads to the presence of rotationally "warm" molecules absorbing the IR light along its path that have to be taken into account for the analysis of spectra and to extract the rotational temperature of the water vapor in the cold part of the supersonic expansion.

The hydrodynamic characteristics of the first cell of the jet, delimited by the nozzle exit and the normal shock wave located about 20 mm downstream, have been extracted from the Pitot probe measurements using the so-called Rayleigh formula.[23] Strictly speaking, this procedure only applies within the assumption of continuous flows, i.e., flows characterized by a Knudsen number (Kn) lower than 0.01. Regarding the present approach, the Kn can be defined as the ratio between the mean-free path of the expanding molecules and the outer diameter of the Pitot probe. As displayed in Figure 3b, Kn attains a value of 0.125 just before the shock wave, which denotes a rarefied regime still far from the free molecular flow regime (Kn > 10). It seems appropriate therefore to use this means of characterization for our free-jet expansion issued from a very narrow width. Note that the values returned by the Rayleigh formula are not correct beyond the shock wave, which is a source of entropy. The Mach number (Figure 3c) attains values up to about 17 in the IR probed zone, revealing an important enthalpy conversion into kinetic energy, thus yielding very low translational temperatures, as can be seen in panel (d). The translational temperature is 3.4 K close to the optical axis, which is located 5 mm downstream from the nozzle. The Pitot probe measurements have been compared to the isentropic model established on the basis of the method of characteristics.[24] Calculated and measured temperatures are remarkably close, thus confirming the validity of the measurements returned by the Pitot probe. In the presence of water vapor, the translational temperature is expected to reach slightly higher values. Indeed, adding a polyatomic molecule in the carrier gas modifies the hydrodynamics by decreasing the

DOI: 10.1021/acs.jpca.7b06858
J. Phys. Chem. A XXXX, XXX, XXX−XXX

Table 1. Experimental Conditions

carrier gas			H_2O			P_{H_2O}, hPa	P_0,[b] hPa	P_{ch},[c] hPa	d^*,[d] μm	T_{rot}(O/P),[e] K	NL_{cold},[f] 10^{14} molec/cm^2	T_{hot},[g] K	NL_{hot},[f] 10^{14} molec/cm^2	τ_{hyd},[h] μs	x_{cond},[i] %
slm															
Ar	He	O_2	g/h	slm	x[a]%										
20			2	0.041	0.21	1.73	843	0.71	36	10.7 ± 1.6/–	1.1 ± 0.3	–	–	8.8	75
20			4	0.083	0.41	3.46	843	0.71	36	9.8 ± 0.6/–	3.0 ± 0.5	–	–	8.8	65
20			8	0.166	0.82	6.94	843	0.71	36	11.6 ± 0.3/13.4 ± 2.7	4.3 ± 0.3	288 ± 50	5.2 ± 0.1	8.8	75
20			10	0.238	1.04	8.68	843	0.71	36	12.0 ± 0.6/12.7 ± 0.5	4.8 ± 0.2	167 ± 13	5.6 ± 0.1	8.8	78
20			12	0.249	1.23	10.37	843	0.71	36	13.0 ± 0.6/13.3 ± 0.1	6.0 ± 0.6	176 ± 30	5.6 ± 1.0	8.8	77
20			20	0.415	2.03	17.15	845	0.71	36	20.2 ± 0.5/18.9 ± 0.4	11.8 ± 1.3	225 ± 25	10.2 ± 1.4	8.8	72
20			30	0.622	3.01	25.68	853	0.72	36	22.4 ± 0.3/24.1 ± 1	15.3 ± 0.7	257 ± 15	17.6 ± 2.4	8.8	76
30			20	0.415	1.36	16.35	1202	1.04	36	18.9 ± 1.3/18.7 ± 0.4	8.8 ± 0.8	–	–	8.8	78
30			50	1.037	3.34	51.20	1533	1.09	18	25.3 ± 0.6/25.7 ± 1.3	13.5 ± 1.5	237 ± 13	28.4 ± 2.2	8.8	79
30			100	2.074	6.47	102.74	1588	1.11	18	32.3 ± 0.4/31.9 ± 0.4	22.2 ± 1.7	251 ± 11	53.5 ± 1.7	8.8	83
		20	8	0.166	0.82	8.88	1083	0.69	18	31.3 ± 0.5/30.4 ± 4	10.4 ± 0.1	–	–	6.6	0
20		20	8	0.166	0.41	8.25	2013	1.33	18	21.8 ± 2/18.0 ± 4	7.8 ± 1.2	–	–	7.6	0
	30		4	0.083	0.28	1.54	549	1.11	36	41.8 ± 3/39.7 ± 4	3.8 ± 0.2	–	–	2.8	0

[a]Water vapor/carrier gas molar ratio. [b]Stagnation pressure. [c]Residual pressure in the expansion chamber. [d]Nozzle width (the slit length is 60 mm). [e]Rotational temperature extracted from *ortho* (O) or *para* (P) rovibrational lines. [f]Column densities for hot and cold gases (see text for details). [g]Rotational temperature of the warm residual gas in shear layers. [h]Hydrodynamic time. [i]Fraction of condensed water vapor.

DOI: 10.1021/acs.jpca.7b06858
J. Phys. Chem. A XXXX, XXX, XXX−XXX

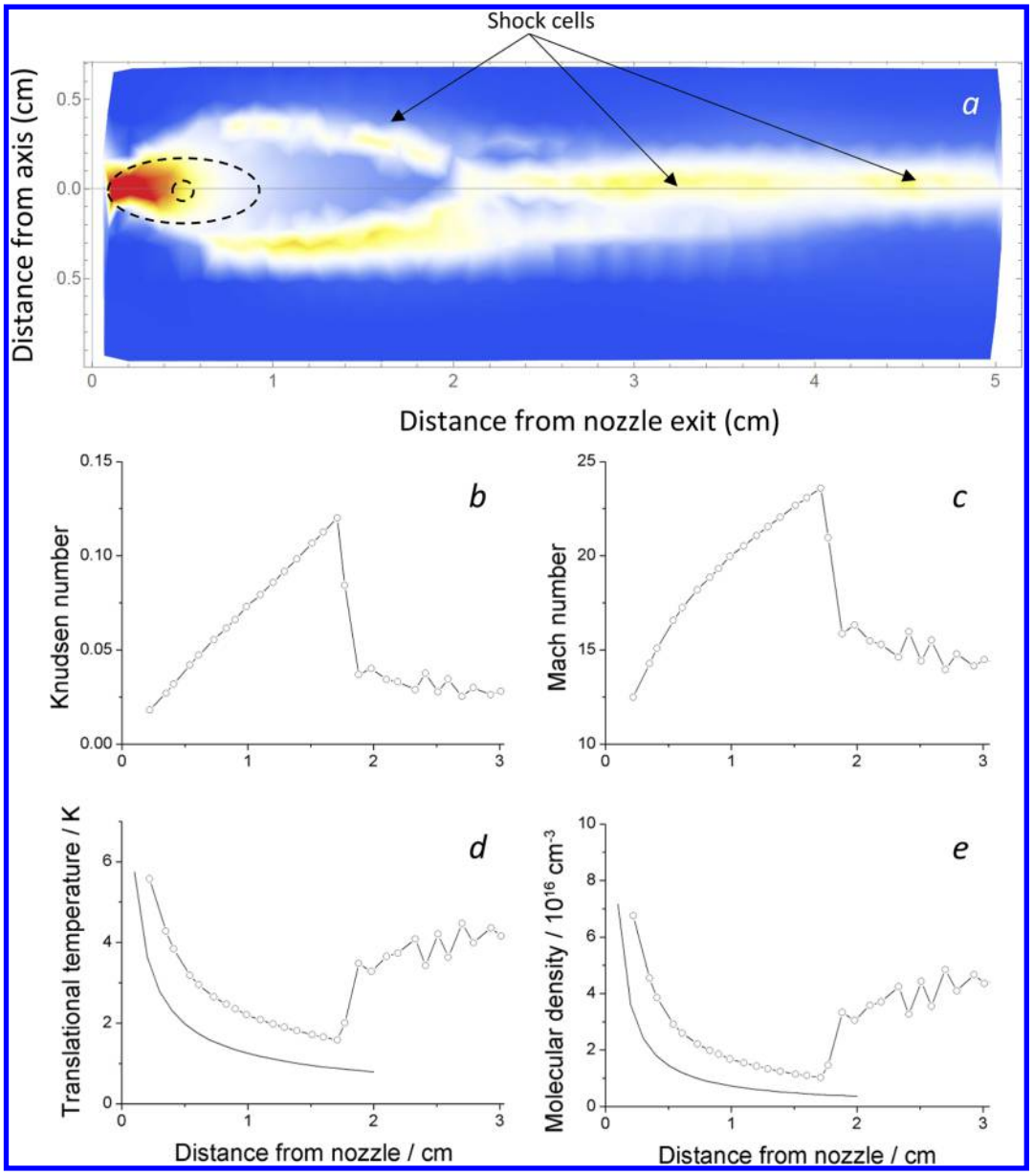

Figure 3. Impact pressure measured by a Pitot probe (a). This 2D map was used to visualize the flow structure in a section perpendicular to the long edge of the slit, resulting from an expansion of argon under conditions very similar to those used for the spectral recordings (P_0 = 1072 hPa, P_{ch} = 0.683 hPa, T_0 = 295 K, slit width: 18 μm, slit length: 60 mm). The path of the IR beam is indicated by the dashed lines (circle = focal point; ellipse = edges of the slit). Various flow parameters have been extracted from measurements relative to the plane of symmetry: Kn (b); Mach number (c); translational temperature (d) compared to a calculation using the method of characteristics (solid line); molecular density (e) compared to a calculation using the method of characteristics (solid line).

specific heat ratio of the mixture, and consequently, the Mach number increase is smaller (some internal energy remains stored in the internal degrees of freedom of the water molecules). The main reason, however, originates from thermodynamics: the condensation heat released by the clustering of water molecules is high and causes very significant warming of the flow, as can be seen from Table 1. Another important parameter of the flow field is its molecular density (Figure 3e). As for the temperature, the molecular density drop associated with our free-jet expansion is extremely abrupt, evolving from 1.7×10^{19} cm^{-3} at the nozzle exit to 3.4×10^{16} cm^{-3} at the optical axis location. It is therefore expected that most of the relaxation processes as well as cluster formation that rely on molecular collisions occur mainly very close to the nozzle exit where the molecular density is still high.

The hydrodynamic time, denoted τ_{hyd} and defined as the time needed by the gas to reach the optical axis from the nozzle exit, can be easily estimated. In a free-jet, the gas reaches its limit velocity v_∞ very rapidly downstream from the nozzle, i.e., after covering a distance equivalent to only a few slit widths. The limit velocity corresponds to a complete conversion of the enthalpy of the gas into kinetic energy (Mach number $M \rightarrow \infty$; flow temperature $T \rightarrow 0$ K), and it is then easily retrieved from the conservation of energy equation,[25] $v_\infty = (2c_pT_0)^{1/2}$, where c_p is the heat capacity at constant pressure of the carrier gas and T_0 is the stagnation temperature, fixed at 313 K in the present study. The value obtained for a flow of argon is 570 m/s, which

DOI: 10.1021/acs.jpca.7b06858
J. Phys. Chem. A XXXX, XXX, XXX−XXX

is remarkably close to the value of 558 m/s calculated from the Mach number and the temperature extracted from the Pitot probe measurement ($v = aM$, where $a = \sqrt{\gamma r T}$ is the speed of sound, γ is the specific heat ratio, and r is the specific gas constant), thus validating the $T \rightarrow 0$ K approximation. Hence, the hydrodynamic times associated with helium, oxygen, and argon are 2.8, 6.6, and 8.8 μs, respectively. These values are slightly overestimated as the heat of water condensation released in the flow adds a supplement of enthalpy into the flow, which can be converted into additional kinetic energy.[26] One should keep in mind that these hydrodynamics times are smaller by several orders of magnitude than the time scale of milliseconds relative to *ortho*−*para* conversion in the condensed phase.[9−11]

WATER CLUSTERING

Figure 2 shows that the rotational temperature steadily increases as the water vapor molar fraction increases in the expansion. This can be understood in terms of the progressive clustering of water molecules that results in a release of more latent heat when a more notable portion of a gas in a mixture condenses. The rotational temperature achieved by the water molecules in the expansion is not only governed by the condensation process. The specific heat ratio of the carrier gas is also an important parameter to consider as it defines the Mach number evolution of the expanding flow for a given nozzle geometry. Thus, compared to a monatomic gas expansion, the expansion of a diatomic gas is characterized by a lower cooling rate (i.e., a smaller Mach number increase) and therefore by a higher translational temperature. The rotational temperature of the water molecules is obviously limited by the "translational bath". As an example, the rotational temperature achieved during our measurements in an expansion of pure oxygen was 31.2 ± 0.6 K, whereas no water clustering was detected on the low-resolution spectrum. For completeness, it should be noted that the rotational relaxation phenomenon depends on the stagnation pressure and the nature of the collision partner. In this respect, helium is far less efficient than argon for inducing $R-T$ energy transfer. Moreover, as the rotational relaxation is proportional to $P_0 d^*$ (see, e.g., ref 27), where P_0 is the stagnation pressure and d^* the slit width, a large stagnation pressure is required for efficient relaxation. However, as helium is lighter than argon by a factor of 10, the same molar flow of helium would lead to a stagnation pressure of about $\sqrt{10} \approx 3$ times lower than that for argon. For these reasons (low $R-T$ energy transfer and low stagnation pressure), the use of helium was rejected in favor of argon. As an example, the maximum flow rate tolerable by our pumping unit (30 slm) was used to inject helium together with a very small amount of water (0.28%), leading to a rotational temperature of around 42 K. As for oxygen, no water clustering was observed.

The extent of water clustering was estimated by comparing the water monomer density *measured* in the cold region of the jet to the monomer density *calculated* assuming no clustering. The way the monomer density was extracted from our high-resolution absorption spectra is explained in detail in the next section, while the calculation was performed using the standard isentropic model equations. More explicitly, the local molecular density N_{jet} of the flow is expressed as a function of the Mach number

$$\frac{N_{jet}}{N_0} = \left(1 + \frac{\gamma - 1}{\gamma} M^2\right)^{1/(1-\gamma)} \quad (1)$$

where N_0 is the total molecular density in the reservoir. For a free-jet expansion, the Mach number is modeled using the following analytical expression

$$M = \delta^{(\gamma-1)/2} \sum_{i=0}^{i=3} \frac{A_i}{\delta^i} \quad (2)$$

Here $\delta = x/d^*$ is the dimensionless distance from the nozzle exit. The various A_i coefficients can be found in ref 28. The calculated water monomer density is given by $x_{H_2O} N_{jet}$. As shown in Figure 4, water condensation reaches 80% when argon is used as carrier gas, revealing, therefore, intense water clustering.

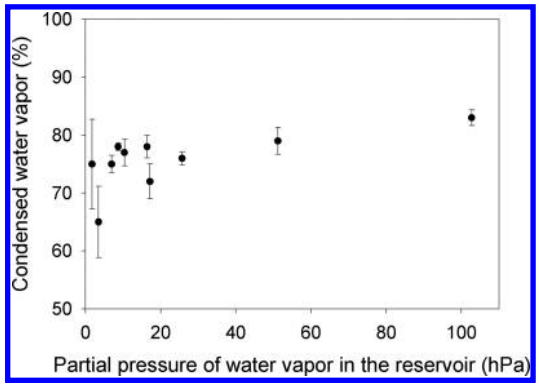

Figure 4. Concentration of condensed water vapor in an expansion of argon. These values, estimated from the measured monomer absorption, reveal a strong water condensation (between 65 and 83%) even for small partial pressures of water vapor.

EXTRACTION OF THE ROTATIONAL TEMPERATURE FROM SPECTROSCOPIC DATA

Our aim was to determine the behavior of the *OPR* under various experimental conditions. The use of high resolution (0.002 cm^{-1}) makes it possible to accurately fit the observed line profiles and retrieve the fractional populations relative to the rotational energetic levels of the *ortho* and *para* molecules. It is then currently possible to determine the rotational temperature T_{rot} of the molecules in the line-of-sight of the IR light beam. To take into account instrument effects inherent to the Fourier transform spectroscopic technique,[29] we analyzed the so-called experimental spectral absorptance (sometime called spectral absorption[30]) denoted $\alpha(\tilde{\nu})$ as per the recommendation of IUPAC.[31] Under that in our experimental conditions,[20] layers of hot gas surround the cold gas and contribute significantly to the total absorptance of the IR light. In the limit of our experimental accuracy, we extracted the integrated Napierian absorbance associated with the two gaseous zones assuming that the medium can be described by a simplified warm/cold bimodal model. Analysis of the rotational populations allowed us to estimate a rotational temperature for the warm gas and for the cold gas. The relative integrated absorbances obtained for four *ortho* lines and one *para* line in the cold gas allow to explore the behavior of the *OPR* of water within the fast slit-jet expansion. In the following,

DOI: 10.1021/acs.jpca.7b06858
J. Phys. Chem. A XXXX, XXX, XXX−XXX

Table 2. Assignments and Some Parameters of the H_2O Absorption Lines of the ν_3 Band Used in This Work

transition	spin−isomer	line position,[a] cm^{-1}	lower energy level,[a] cm^{-1}/K	line intensity, 10^{-19} S_{fi}^{N},[a] cm/molec	line strength, $10^{18}F_{fi}^{N}$, cm/molec
$1_{01} \leftarrow 2_{02}$	*para*	3709.40227	70.0908/100.8457	0.702	3.44721
$1_{10} \leftarrow 1_{11}$	*para*	3759.84448	37.1371/53.4324	0.5809	4.05056
$1_{01} \leftarrow 0_{00}$	*para*	3779.49307	0	0.4559	7.96176
$2_{12} \leftarrow 1_{11}$	*para*	3796.43951	37.1371/53.4324	0.5527	3.85393
$3_{03} \leftarrow 2_{02}$	*para*	3820.73852	70.0908/100.8457	0.8754	4.29869
$1_{11} \leftarrow 2_{12}$	*ortho*	3712.20451	79.4964/114.3783	1.501	2.57184
$0_{00} \leftarrow 1_{01}$	*ortho*	3732.13435	23.7944/34.2351	1.303	2.83838
$1_{11} \leftarrow 1_{10}$	*ortho*	3749.32915	42.3717/60.9638	1.743	4.15566
$2_{11} \leftarrow 2_{12}$	*ortho*	3769.88893	79.4964/114.3783	0.7786	1.33407
$2_{02} \leftarrow 1_{01}$	*ortho*	3801.41863	23.7944/34.2351	2.312	5.03633
$2_{11} \leftarrow 1_{10}$	*ortho*	3807.01357	42.3717/60.9638	1.562	3.72412
$3_{13} \leftarrow 2_{12}$	*ortho*	3816.09164	79.4964/114.3783	2.312	3.96143
$2_{20} \leftarrow 1_{01}$	*ortho*	3863.31982	23.7944/34.2351	0.0456	0.09933

[a]From ref 32.

we describe the procedure used to retrieve the parameters characterizing the cold part of the expansion.

The absorptance $\alpha(\tilde{\nu})$ is obtained by comparing the spectral intensity of light $I(\tilde{\nu})$ at the output of the chamber to the intensity of light at its entrance $I_0(\tilde{\nu})$

$$\alpha(\tilde{\nu}) = \Delta I(\tilde{\nu})/I_0(\tilde{\nu}) = (I_0(\tilde{\nu}) - I(\tilde{\nu}))/I_0(\tilde{\nu}) \quad (3)$$

$I(\tilde{\nu})$ follows the Beer−Lambert law and is given by

$$I(\tilde{\nu}) = I_0(\tilde{\nu}) \exp(-A_{fi} \times V(\tilde{\nu})) \quad (4)$$

where A_{fi} is defined as the integrated Napierian absorbance of the line for a transition from a state i to a state f and $V(\tilde{\nu})$ is a normalized line profile (generally a Voigt profile taking into account inhomogeneous Doppler broadening and homogeneous collisional broadening).

A_{fi} is given by the following equation[32,33]

$$A_{fi} = \int \sigma(\tilde{\nu}) NL \, d\tilde{\nu} \quad (5)$$

where $\sigma(\tilde{\nu})$ is the absorption cross section at the wavenumbers $\tilde{\nu}$, L the thickness of the sample, and N is the number of molecules per unit volume. Then, one has

$$A_{fi} = S_{fi}^{N} NL \quad (6)$$

where the integrated absorption cross section of the line (also called the line intensity in refs 32 and 33) S_{fi}^{N} (cm^{-1}/molecules cm^{-2}) is given in the gas phase by

$$S_{fi}^{N} = \frac{8\pi^3}{3hc}\tilde{\nu}_{fi}\left[1 - \exp\left(-\frac{hc\tilde{\nu}}{kT}\right)\right] \times \mathfrak{R}_{fi} \times 10^{-36} \times n_i \quad (7)$$

where T is the temperature, $\mathfrak{R}_{fi}$(Debye^2) is the square of the transition moment, and n_i represents the fractional population in the initial state. At low temperature (below 296 K), the wavenumber $\tilde{\nu}_{fi}$ of the transition is sufficiently high so that the exponential term vanishes. Then

$$S_{fi}^{N} = \frac{8\pi^3}{3hc}\tilde{\nu}_{fi} \times \mathfrak{R}_{fi} \times 10^{-36} \times n_i \quad (8)$$

Finally the integrated Napierian absorbance is related to the fractional population through the simple relation

$$A_{fi} = F_{fi}^{N} NL \times n_i \quad (9)$$

where F_{fi}^{N} is independent of the temperature and afterward will be called the line strength. The evolution of the integrated Napierian absorbance is then directly related to the evolution of the population in the initial state. When the fractional populations of the rotational energy levels follow the thermodynamic equilibrium statistics, the population n_i is given by

$$n_i = \frac{1}{Q(T)} g_i \exp\left(-\frac{hcE_i}{kT}\right) \quad (10)$$

where the energy of the initial level E_i is given in cm^{-1} and T is in K, $Q(T)$ is the partition function, and $g_i = g_{NS}g_J$ with g_{NS} as the degeneracy of the considered nuclear spin state and $g_J = 2J + 1$ as the degeneracy of the rotational state (Zeeman sublevels).

By extracting the integrated Napierian absorbance of the lines A_{fi} under our experimental conditions, it is then possible to extract the rotational temperature T_{rot} using the following linear equation

$$\log(A_{fi}/F_{fi}^{N}/g_J) = \log(NLn_i/(2J + 1)) = -\frac{hc}{k}\frac{E_i}{T} + \log\left(\frac{g_{NS}}{Q(T)}\right) \quad (11)$$

which becomes

$$\log(NLn_i/(2J + 1)) = -\frac{E_i}{T} + \log\left(\frac{g_{NS}}{Q(T)}\right) \quad (12)$$

when the initial energy E_i is expressed in kelvins.

In the spectral region at around 3700 cm^{-1}, the Doppler half width at half maximum (HWHM) ranges between 1×10^{-3} and 5×10^{-3} cm^{-1} for temperatures between 10 and 250 K. It is then necessary to take into account the width of the apparatus function to accurately model the line shape. The width of the apparatus function ($\sim 2 \times 10^{-3}$ cm^{-1}) has to be taken into account to perform accurate analysis of the line shape. Experimentally, the intensity of the light is given by the convolution product

$$I_{exp}(\tilde{\nu}) = I(\tilde{\nu}) * f_{app}(\tilde{\nu}) \quad (13)$$

where the apparatus function $f_{app}(\tilde{\nu})$ is modeled by the Fourier transform of the Boxcar function

DOI: 10.1021/acs.jpca.7b06858
J. Phys. Chem. A XXXX, XXX, XXX−XXX

$$f_{app}(\tilde{\nu}) = \frac{2}{R} \times \mathrm{sinc}\left(\frac{2\tilde{\nu}}{R}\right) \quad (14)$$

Here $\mathrm{sinc}(x) = \frac{\sin(\pi \cdot x)}{\pi \cdot x}$. The resolution R is given by $R = 1/MOPD$, where MOPD is the maximum optical path difference. In our case, the resolution corresponds to the resolution defined by the Bruker company divided by 0.9, and then $R = 2.22 \times 10^{-3}$ cm^{-1}. The experimental absorption becomes

$$\alpha_{exp}(\tilde{\nu}) = \frac{(I_0(\tilde{\nu}) - I(\tilde{\nu})) * f_{app}(\tilde{\nu})}{I_0(\tilde{\nu}) * f_{app}(\tilde{\nu})} \quad (15)$$

For FTIR spectroscopy, the entrance intensity $I_0(\tilde{\nu})$ is spectrally broad compared to the width of the apparatus function. Then, $I_0(\tilde{\nu}) * f_{app}(\tilde{\nu}) \approx I_0(\tilde{\nu})$, and the absorptance is given by

$$\alpha_{exp}(\tilde{\nu}) = ((I_0(\tilde{\nu}) - I(\tilde{\nu})) * f_{app}(\tilde{\nu}))/I_0(\tilde{\nu}) \approx \alpha(\tilde{\nu}) * f_{app}(\tilde{\nu}) \quad (16)$$

then

$$\alpha_{exp}(\tilde{\nu}) = (1 - \exp(-A_{fi} \times V(\tilde{\nu}))) * f_{app}(\tilde{\nu}) \quad (17)$$

The variations of absorption lines intensities have been plotted as a function of T_{rot} for a series of reference lines listed in Table 2.

Because the gas temperature in the shear layers is significantly higher than that in the central part of the jet, more observed rotational lines are due to absorption by the warm gas than by the cold one. We performed the analysis of the individual line shapes based on a two-step procedure that uses a homemade computational code written in MATLAB language:

(i) In the first step, the absorption $\alpha_{exp}(\tilde{\nu})$ of each individual line was fitted using a Gaussian profile $V(\tilde{\nu})$. The only fitted parameters were the integrated Napierian absorbance A_{fi} and the HWHM of the Gaussian profile. For experimental conditions relative to higher water concentrations, contribution from the low-temperature gas could be neglected for transitions originating from an initial energetic level higher than 190 K. Indeed for these transitions, the line shape was perfectly fitted using eq 15 and the rotational diagram shows linear behavior for energy E_i above 190 K (see Figure 5). Application of eq 9 yielded the averaged column density NL^{hot} listed in Table 1 for each line. It should be noted that for the calculation of the population factor n_i appearing in eq 9, the OPR value was assumed to be close to 3. Because of the high temperature considered here, this value is justified by the fact that calculations give values close to 3 irrespective of the nuclear spin equilibration dynamics (fast or slow NSC; see text below and eqs 17−21). Application of eqs 11 and 12 to the same integrated absorbances led to the rotational temperatures T_{hot}, also listed in Table 1. For the case of a flow of 100 g/h of water in 30 slm of Ar, the rotational diagram gives a high rotational temperature $T_{hot} = 251 \pm 11$ K very close to the translational temperature $T = 260 \pm 40$ K extracted from the HWHM Gaussion line shape. For the "low-temperature" lines, the difference between the calculated and experimental spectral absorptance shows a typical residue presented in Figure 6a (the case of the $1_{11} \leftarrow 1_{10}$ transition). For the case of low water concentration, our signal-to-noise ratio was too low to permit detection of high-J rotational lines. Therefore, the only

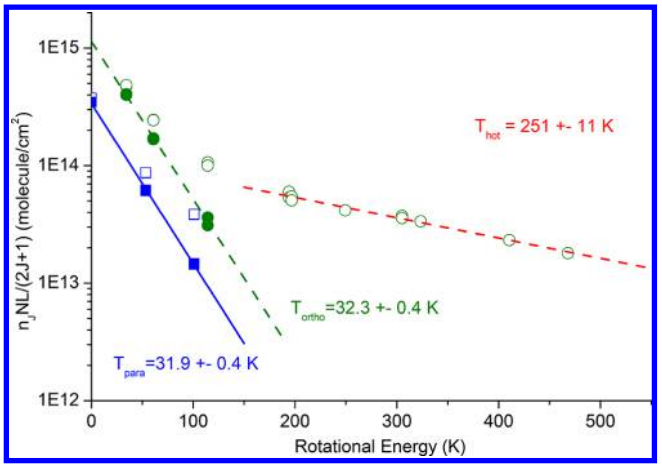

Figure 5. Example of a rotational diagram used to extract the rotational temperature from absorbance spectra in the case of the presence of hot and cold molecules in the path of the IR beam (here 100 g/h of H_2O in 30 slm of argon). The quantity $(NLn_i/(2J + 1))$ (see eq 10) extracted from the fitting of the differents lines is represented as a function of the energy level E_i of the initial state of the transition. The open circles and open squares represent the data obtained with a single Gaussian profile for *ortho* and *para* lines, respectively. The data for energies E_i higher than 190 K follow a straight line, and the slope gives the rotational temperature of the hot molecules (251 ± 11 K). The warm gas contribution is then removed from the low-J rotational line absorption by a fitting procedure taking into account the hot and cold contributions (see text for details), leading to a corrected value of the cold gas rotational temperature for the *ortho* molecules (32.3 ± 0.4 K) very close to the rotational temperature extracted from the lines associated with the *para* molecules (31.9 ± 0.4 K). A total of eight low-J rotational lines have been used to estimate the cold rotational temperature.

observable transitions were those originating from initial energy states E_i lower than 190 K. The rotational diagrams for *ortho* and *para* were linear for energy lower than 190 K. This means that the populations followed a Bolztmann distribution, allowing us to extract rotational temperatures directly using eq 12. The rotational temperatures extracted for the *ortho* and *para* molecules are listed in Table 1.

(ii) In a second step, we focused our analysis on spectra recorded with higher water concentration. We fitted the lines corresponding to transitions related to initial rotational states below 190 K, including the contribution of the warm gas. The absorptance was then fitted using

$$\alpha_{exp}(\tilde{\nu}) = (1 - \exp(-A_{fi}^{cold} \times V^{cold}(\tilde{\nu}) - A_{fi}^{hot} \times V^{hot}(\tilde{\nu}))) * f_{app}(\tilde{\nu}) \quad (18)$$

Figure 6b shows that the discrepancies between the calculated and the experimental absorptances are drastically reduced for a flow of 100 g/h of water in 30 slm of argon. The only parameters in this second step were A_{fi}^{cold} and the HWHM of the Gaussian profile $V^{cold}(\tilde{\nu})$. In this extreme case, the contribution of the hot molecules counts for a third of the total absorbance. We were then able to remove the hot gas contribution from the absorbance of these low-J rotational lines. Figure 5 shows that the populations reported for the cold molecules in the rotational diagram follow a straight line.

In all cases, rotational temperatures for *ortho* and *para* subsystems were determined independently and were found to be nearly equal (see Table 1). The integrated absorbances obtained for the "cold" transitions and the average rotational

DOI: 10.1021/acs.jpca.7b06858
J. Phys. Chem. A XXXX, XXX, XXX−XXX

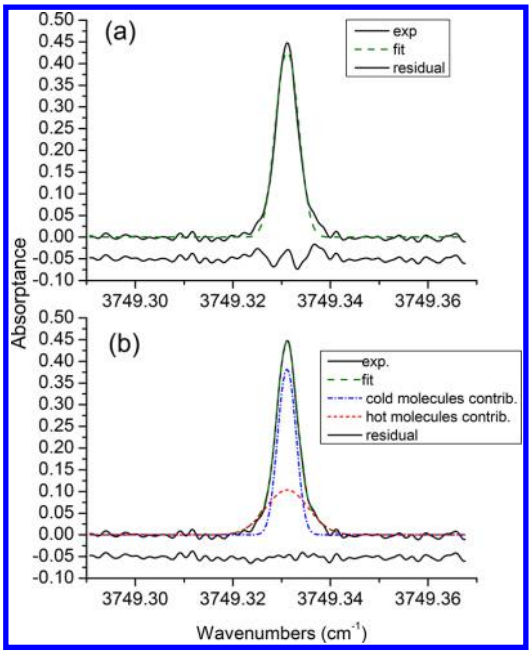

Figure 6. Absorptance of the $1_{11} \leftarrow 1_{10}$ transition observed with a flow of 100 g/h of water in 30 slm of Ar. The experimental data (line) are compared to the calculated data (dasedh line) after a fitting procedure (a) with a single Gaussian profile and (b) with two Gaussian profiles associated with one contribution coming from "hot" gas (red dash lines) and one contribution from "cold" gas (blue short dash−dot line) convoluted by the appropriate apodization function (Boxcar). The obs−calc residue is depicted in the bottom part of each panel.

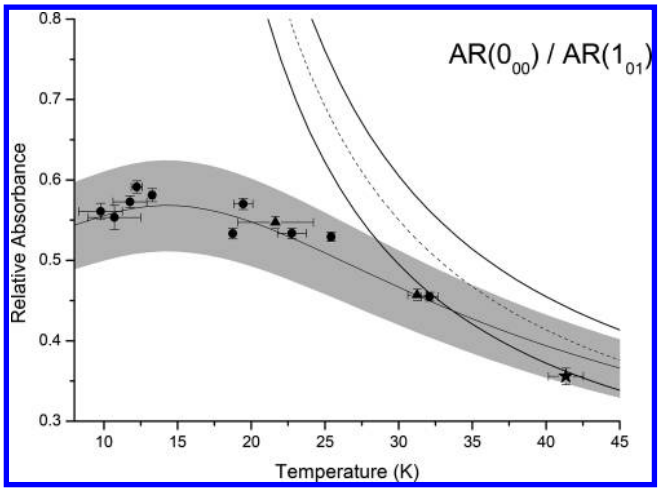

Figure 7. Relative integrated absorbances $A_{1_{01}\leftarrow 0_{00}}/A_{2_{02}\leftarrow 1_{01}}$ measured as a function of rotational temperature. The expected behavior in the case of slow NSC (solid line) and that in case of fast NSC (dashed line) are also represented. An uncertainty of 10% on the theoretical values is shown in gray, derived from HITRAN[32] data. Triangle symbols represent data obtained in pure oxygen or in a mixture with equal Ar and O_2 flow rates as a carrier gas, as shown in Table 3, whereas the star refers to the data obtained in an expansion of He instead of Ar as a carrier gas. The *x*-axis error bars reflect the uncertainty of the rotational temperature retrieved from the rotational diagram. The *y*-axis error bars originate from the most severe estimate of uncertainty in the line intensity measurements following subtraction, when possible, of the hot gas contribution to the low-temperature line absorption.

temperatures in the various experimental conditions are listed in Table 3. Figures 7−10 show the evolution of the *otho*/*para* relative absorbances for several transitions as a function of rotational temperature. As these ratios indicate that the *OPR* has not been relaxed during the cooling down, we calculated the n_i fractional population using a conversion factor $(CF)_{slow}$ as described by eq 23. The NL^{cold} column densities estimated for the cold gas in various conditions are reported in Table 3 and can be compared to the warm gas contribution NL^{hot}. They have been used to estimate the fraction of condensed water.

Finally, we evaluated a possible contribution of homogeneous collisional broadening under the conditions of pressure and temperature of our experiment using the broadening coefficients tabulated in the HITRAN database.[32] Under the various experimental conditions used in this work, the collisional width was always less than 10^{-7} cm^{-1} (HWHM), justifying a posteriori the use of a Gaussian profile for the line shape analysis.

Although the IR light beam diameter is rather large compared to the flow field dimension, two well-defined low- and high-rotational temperatures could be extracted from our

Table 3. Rotational Temperatures T_{rot} and Integrated Napierian Absorbances *A* Associated with the Molecules Present in the Cold Part of Supersonic Expansion

carrier gas/slm			H_2O, g/h	T_{rot}[a], K	$AR(0_{00})$,[b] 10^{-3}	$AR(1_{01})$,[c] 10^{-3}	$AP(1_{01})$,[d] 10^{-3}	$AQ(1_{10})$,[e] 10^{-3}	$AR(1_{10})$,[f] 10^{-3}
Ar	He	O_2			*para*	*ortho*	*ortho*	*ortho*	*ortho*
20			2	10.7 ± 1.8	0.754 ± 0.014	0.792 ± 0.012	1.36 ± 0.03	0.084 ± 0.004	0.067 ± 0.008
20			4	9.8 ± 1.5	1.56 ± 0.02	1.65 ± 0.02	2.78 ± 0.03	0.169 ± 0.006	0.178 ± 0.007
20			8	11.8 ± 1.2	2.21 ± 0.02	2.32 ± 0.02	3.86 ± 0.04	0.336 ± 0.007	0.316 ± 0.009
20			10	12.2 ± 0.4	2.58 ± 0.02	2.64 ± 0.02	4.36 ± 0.04	0.397 ± 0.007	0.374 ± 0.008
20			12	13.3 ± 0.2	2.74 ± 0.02	2.87 ± 0.03	4.72 ± 0.05	0.499 ± 0.010	0.478 ± 0.006
20			20	19.5 ± 0.7	3.31 ± 0.02	3.53 ± 0.03	5.82 ± 0.06	1.10 ± 0.01	1.010 ± 0.008
20			30	22.8 ± 1.0	3.36 ± 0.02	3.69 ± 0.03	6.31 ± 0.06	1.56 ± 0.01	1.45 ± 0.01
30			20	18.8 ± 0.1	2.33 ± 0.02	2.53 ± 0.03	4.37 ± 0.04	0.825 ± 0.018	0.749 ± 0.016
30			50	25.4 ± 0.2	2.69 ± 0.02	2.94 ± 0.02	5.07 ± 0.04	1.29 ± 0.01	1.20 ± 0.01
30			100	32.1 ± 0.4	2.77 ± 0.02	3.49 ± 0.03	6.09 ± 0.06	2.16 ± 0.02	2.01 ± 0.02
		20	8	31.2 ± 0.6	1.25 ± 0.02	1.59 ± 0.02	2.75 ± 0.02	0.978 ± 0.016	0.884 ± 0.016
20		20	8	21.6 ± 2.6	1.90 ± 0.02	1.92 ± 0.03	3.48 ± 0.03	0.690 ± 0.014	0.703 ± 0.018
	30		4	41.3 ± 1.2	0.28 ± 0.01	0.451 ± 0.006	0.786 ± 0.008	0.330 ± 0.007	0.328 ± 0.008

[a]Average rotational temperature. [b]$1_{01} \leftarrow 0_{00}$. [c]$2_{02} \leftarrow 1_{01}$. [d]$0_{00} \leftarrow 1_{01}$. [e]$1_{11} \leftarrow 1_{10}$. [f]$2_{11} \leftarrow 1_{10}$ transitions.

DOI: 10.1021/acs.jpca.7b06858
J. Phys. Chem. A XXXX, XXX, XXX−XXX

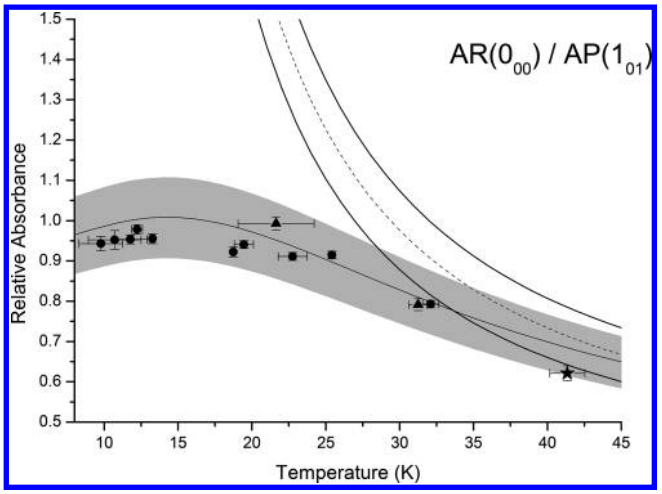

Figure 8. Relative integrated absorbances $A_{1_{01}\leftarrow 0_{00}}/A_{0_{00}\leftarrow 1_{01}}$ measured as a function of rotational temperature. See the Figure 7 caption for more details.

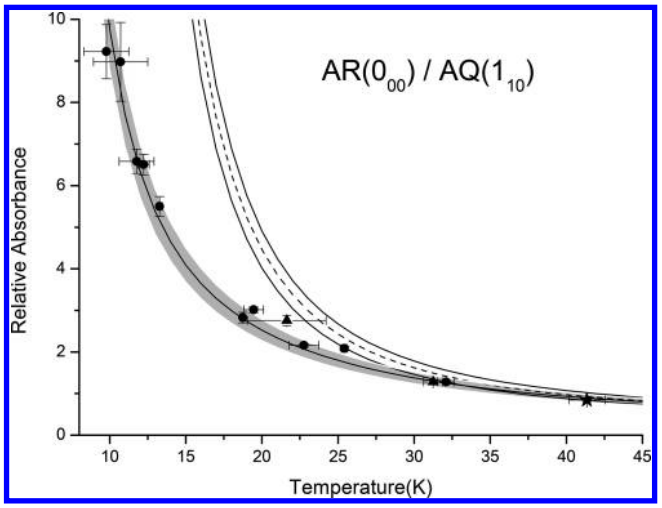

Figure 9. Relative integrated absorbances $A_{1_{01}\leftarrow 0_{00}}/A_{1_{11}\leftarrow 1_{10}}$ measured as a function of rotational temperature. See the Figure 7 caption for more details.

spectra using the above two-step procedure, which seems contradictory regarding the density and temperature gradients highlighted by the Pitot probe measurements (see Figure 3). In the zone of silence, it appears that beyond a certain distance from the nozzle the gas absorption becomes too weak to contribute significantly. Another assumption is that the rotational temperature no longer relaxes beyond a certain distance from the nozzle due to a lack of collisions.

DISCUSSION

To investigate the behavior of the nuclear spin isomers' spin species after the fast expansion, we followed the procedure used by Manca Tanner et al.[3] As the experimental data showed that rotational populations of *ortho* and *para* molecules were equilibrated at the same rotational temperature T, we conducted our analysis of the *OPR* using the following method. The ratio of integrated absorbance of one *ortho fi* transition to one *para* $f'i'$ transition is proportional to the ratio of the fractional population of molecules in the two considered rotational states

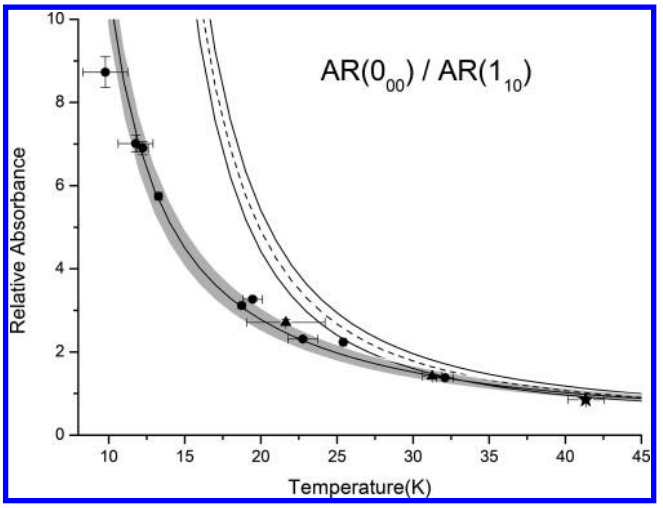

Figure 10. Relative integrated absorbances $A_{1_{01}\leftarrow 0_{00}}/A_{2_{11}\leftarrow 1_{10}}$ measured as a function of rotational temperature. See the Figure 7 caption for more details.

$$\frac{A_{fi}}{A_{f'i'}} = \frac{F^N_{fi}}{F^N_{f'i'}} \times \frac{n_i}{n_{i'}} = \frac{F^N_{fi}}{F^N_{f'i'}} \times \frac{g_i}{g_{i'}} \exp\left(-\frac{hc(E_i - E_{i'})}{kT}\right) \times CF$$

$$\frac{A_{fi}}{A_{f'i'}} = \frac{F^N_{fi}}{F^N_{f'i'}} \times \frac{g_{\mathrm{NS}_i} g_{J_i}}{g_{\mathrm{NS}_{i'}} g_{J_{i'}}} \exp\left(-\frac{hc(E_i - E_{i'})}{kT}\right) \times CF \quad (19)$$

where $g_{\mathrm{NS}} = 2I + 1$ is the nuclear spin state degeneracy given for a value of the total nuclear spin momentum number I and CF is a conversion factor.

OPR is a key parameter for our analysis. The *OPR* at a temperature T can be defined assuming that the *ortho* and *para* molecules behave as independent species (however both in contact with the same thermal bath of the expanding gas).[34] It can be calculated from separate partition functions evaluated for each nuclear spin conformer $Q_{ortho}(T)$ and $Q_{para}(T)$ expected at thermal equilibrium. When the $OPR(T)$ is out of equilibrium but the rotational *ortho* and *para* subsystems are equilibrated, the coefficient of proportionality between the total *ortho* fractional populations n_{ortho} and $Q_{ortho}(T)$ is different than the one between n_{para} and $Q_{para}(T)$. The CF in eq 19 is then given by

$$OPR(T) = \frac{Q_{ortho}(T)}{Q_{para}(T)} \times CF = \frac{\sum g_{\mathrm{NS}}(ortho) g_J(ortho) \exp\left(-\frac{hcE_{ortho}}{kT}\right)}{\sum g_{\mathrm{NS}}(para) g_J(para) \exp\left(-\frac{hcE_{para}}{kT}\right)} \times CF \quad (20)$$

Here and below the summation extends to all of the *ortho* or *para* lines. Two limiting cases can be distinguished.

(i) In the case of Fast NSC (designated by Fast in the following), the equipartition of the nuclear spin states gives a $(CF)_{\mathrm{Fast}}$ factor equal to 1. As a result, eq 20 becomes

$$OPR(T) = 3\frac{\sum g_J(ortho) \exp\left(-\frac{hcE_{ortho}}{kT}\right)}{\sum g_J(para) \exp\left(-\frac{hcE_{para}}{kT}\right)} \quad (21)$$

DOI: 10.1021/acs.jpca.7b06858
J. Phys. Chem. A XXXX, XXX, XXX−XXX

(ii) In the case of Slow NSC (Slow in the following), we assume that the total number of molecules in each nuclear spin configuration remains constant during the cooling. Starting from a gaseous mixture with an *OPR* of 3, the ratio of the absorbances has to be calculated with a temperature-dependent $(CF)_{\mathrm{Slow}}$ parameter imposing an $OPR(T) = 3$ irrespective of the temperature

$$OPR(T) = 3(CF)_{\mathrm{Slow}} \times \left(\frac{\sum g_J(ortho) \exp\left(-\frac{hcE_{ortho}}{kT}\right)}{\sum g_J(para) \exp\left(-\frac{hcE_{para}}{kT}\right)} \right) = 3 \tag{22}$$

thus giving

$$(CF)_{\mathrm{Slow}} = 1/\left(\frac{\sum g_J(ortho) \exp\left(-\frac{hcE_{ortho}}{kT}\right)}{\sum g_J(para) \exp\left(-\frac{hcE_{para}}{kT}\right)} \right) \tag{23}$$

$(CF)_{\mathrm{Slow}}$ is calculated using eq 23 to determine the theoretical ratio $A_{fi}/A_{f'i'}$ between absorbances of two transitions in the case of Slow NSC. In the section below, we shall compare the measured ratios of integrated absorption for selected pairs of *ortho* and *para* transitions with what can be expected for the limiting Fast or Slow NSC cases.

The theoretical ratio of integrated absorbances $A_{fi}/A_{f'i'}$ was calculated using either eq 19 into which the CF parameter was substituted assuming it equals 1 in the case of Fast conversion or eq 23 in the case of Slow conversion. The values of the J quantum number, the energy of the low-lying level of a selected transition, and the line intensities $S_{fi}^{N}(296\ \mathrm{K})$ were taken from the HITRAN database.[32] Note that the line strengths F_{fi} that enter eq 19 were calculated from line intensities $S_{fi}^{N}(296\ \mathrm{K})$ reported in Table 2. The error is between 5 and 10%, which gives an uncertainty of 10−20% on the relative absorbances.

Then the calculated values of $A_{fi}/A_{f'i'}$ were compared with the ratio of absorbances retrieved from the fit of experimentally recorded line profiles and given in Table 3. Comparison between experimental measurements and expected values are presented in Figures 7−10. Confidence domains presented in these figures for the theoretical values in the case of Fast or Slow NSC are calculated using 10% error given by the uncertainties on line intensities $S_{fi}^{N}(296\ \mathrm{K})$ reported in the HITRAN Database.[32]

Figures 7−10 show that in all cases our measured ratios of integrated absorbances are in agreement with an assumption of Slow NSC. It is seen that even the use of oxygen instead of argon as a carrier gas does not result in the change of the NSC rate. We do not observe any effect of cluster formation on the change in the NSC rate as was suggested in ref 3, despite clear evidence of cluster signatures in our recorded low-resolution spectra and an important fraction of condensed water molecules, as estimated from our high-resolution spectra. The rate of water condensation in an expansion of argon was estimated by comparing the monomer concentration extracted from the line absorbances to the value given by the isentropic model for which a total absence of condensation is assumed. As shown in Figure 4, water condensation reaches 80% when argon is used as the carrier gas, revealing, therefore, intense water clustering. Under our experimental conditions, a fast NSC would then be expected even at low temperature when the two models give very different *ortho*/*para* intensity ratios. Figures 7−10 show that such an effect does not occur. One explanation could arise from the expansion dynamics differing between our study and that performed by Manca Tanner et al.[3] At first glance, the differences are quite subtle. Indeed, the flow characteristics in the isentropic part of a supersonic expansion are governed by only a few parameters linked to the nozzle geometry and the stagnation conditions (namely, temperature, pressure, specific heat ratio of the expanding mixture, water molar fraction). It appears that in both studies a slit nozzle has been used, argon was mainly used, and very similar stagnation pressures and temperatures have been set, so that very similar flow expansions are therefore expected. One has to notice, however, that the wider 100 μm width nozzle used in ref 3 (versus 18 and 36 μm in the present work) certainly leads to a slightly lower cooling rate. However, as in this former study, the flow was probed farther from the nozzle exit (10 vs 5 mm), and the temperature and molecular density reached by the flow for equivalent gas compositions are expected to be very similar to those obtained in the present work. However, it is interesting to notice that the extracted rotational temperature is systematically higher by about 5 K for equivalent partial pressures of water (see Table 6 of ref 3). One explanation could be attributed to more pronounced water condensation induced by the wider slit nozzle used in ref 3. Finally, to be complete, one has to point out a hydrodynamic time (as defined previously) two times larger in ref 3 (~18 vs ~9 μs) because of the larger probing distance. We are considering using a Laval nozzle to better control water clustering and to increase the hydrodynamic time (see, e.g., ref 35). It would provide us with new insights on the effects of the hydrodynamic time and the rate of water condensation in the expansion.

CONCLUSIONS

The present paper was aimed at a further examination of water vapor nuclear spin isomerization. In recent years, the mechanism and the effectiveness of NSC among water vapor *ortho* and *para* spin isomers have been the subject of a number of studies that often gave rise to contradictory conclusions. We have conducted a jet-FTIR examination of several water vapor absorption lines seen in H_2O seeded expansions using pure argon or helium as carrier gases. Some experiments were carried out with dioxygen as the carrier gas or coadded to an expanding mixture of gases in order to accelerate *ortho*−*para* conversion due to collisions with paramagnetic oxygen molecules. To summarize, we did not observe any signs of nuclear spin relaxation in the wide range of expansion conditions that were used:

- H_2O molar fraction: from 0.2 to 6.5%;
- rotational temperature range: from 10 to 42 K;
- transitions explored: one *para* line ($1_{01} \leftarrow 0_{00}$) and four *ortho* lines ($2_{02} \leftarrow 1_{01}$; $0_{00} \leftarrow 1_{01}$; $1_{11} \leftarrow 1_{10}$; $2_{11} \leftarrow 1_{10}$).

In any event, the measured *OPR* corresponded to the temperature in the stagnation reservoir and was not relaxed to very low rotational temperatures measured at the sampled volume of the jet. Moreover, despite clear signatures of water clusters that were formed at some experimental conditions, we did not observe any effect of clustering on the rate of nuclear spin isomer conversion. This result agrees with a conclusion that has been drawn from a similar experiment in ref 15 and differs significantly from what has been reported previously by ref 3. On the basis of the results obtained, we are in a position to state that at least the suggestion of ref 3 that the transition

DOI: 10.1021/acs.jpca.7b06858
J. Phys. Chem. A XXXX, XXX, XXX−XXX

from nuclear spin conservation to nuclear spin relaxation regimes is due to clustering in an expansion is not supported by our measurements, also in agreement with the previous work.[15]

AUTHOR INFORMATION

Corresponding Author

*E-mail: robert.georges@univ-rennes1.fr.

ORCID

Robert Georges: 0000-0003-4885-1536
Pierre Asselin: 0000-0002-2526-8260
Thérèse Huet: 0000-0001-9104-5156
Martin Fournier: 0000-0002-8771-3913

Notes

The authors declare no competing financial interest.

ACKNOWLEDGMENTS

The authors are grateful to SOLEIL and the AILES staff for providing technical support under the proposal 20120156. X.M. and A.M. are grateful to the French National Research Agency (Project ANR GASOSPIN No. 09-BLAN-0066-01) for the financial support of the calculation code development. A.V. acknowledges partial support from the RFBR Grant 15-05-00736 and the Russian Acad. Sci. Program 7. This work was supported by the Programme National "Physique et Chimie du Milieu Interstellaire" (PCMI) of CNRS/INSU with INC/INP cofunded by CEA and CNES. The authors warmly thank the reviewers for their valuable comments and suggestions, which have helped to improve the quality of our manuscript.

REFERENCES

(1) Cacciani, P.; Cosléou, J.; Khelkhal, M. Nuclear Spin Conversion in H_2O. *Phys. Rev. A: At., Mol., Opt. Phys.* **2012**, *85*, 012521/1−012521/8.

(2) Chapman, W. B.; Kulcke, A.; Blackmon, B. W.; Nesbitt, D. J. Rotationally Inelastic Scattering of Jet Cooled H_2O with Ar: State-to-State Cross Sections and Rotational Alignment Effects. *J. Chem. Phys.* **1999**, *110*, 8543−8554.

(3) Manca Tanner, C.; Quack, M.; Schmidiger, D. Nuclear Spin Symmetry Conservation and Relaxation in Water ($^1H_2^{16}O$) Studied by Cavity Ring-Down (CRD) Spectroscopy of Supersonic Jets. *J. Phys. Chem. A* **2013**, *117*, 10105−10118.

(4) Konyukhov, V. K.; Tikhonov, V. I.; Tikhonova, T. L.; Faizulaev, V. N. Separation of Spin-Modifications of Water and Heavy-Water Molecules. *Pis'ma v Zhurnal Tekhnicheskoi Fiziki* **1986**, *12*, 1438−1441. [in Russian].

(5) Tikhonov, V.; Volkov, A. Separation of Water into its *ortho* and *para* Isomers. *Science* **2002**, *296*, 2363.

(6) Stepanov, E. V.; Tikhonov, V. I.; Milyaev, V. A. Diagnostics of *ortho* and *para* Water Isomers with Tunable Diode Lasers. *Quantum Electron.* **2005**, *35*, 205. [in Russian].

(7) Stepanov, E. V.; Zyryanov, P. V.; Milyaev, V. A. Laser Analysis of the Relative Content of *ortho*- and *para*-Water Molecules for the Diagnostics of Spin-Selective Processes in Gaseous Media. *Phys. Wave Phenom.* **2010**, *18*, 33−43.

(8) Veber, S. L.; Bagryanskaya, E. G.; Chapovsky, P. L. On the Possibility of Enrichment of H_2O Nuclear Spin Isomers by Adsorption. *J. Exp. Theor. Phys.* **2006**, *102*, 76−83.

(9) Buntkowsky, G.; Limbach, H.-H.; Walaszek, B.; Adamczyk, A.; Xu, Y.; Breitzke, H.; Schweitzer, A.; Gutmann, T.; Wächtler, M.; Frydel, J.; et al. Mechanisms of Dipolar Ortho/Para-H_2O Conversion in Ice. *Z. Phys. Chem.* **2008**, *222*, 1049−1063.

(10) Abouaf-Marguin, L.; Vasserot, A.-M.; Pardanaud, C.; Michaut, X. Nuclear Spin Conversion of Water Diluted in Solid Argon at 4.2 K: Environment and Atmospheric Impurities Effects. *Chem. Phys. Lett.* **2007**, *447*, 232−235.

(11) Sliter, R.; Gish, M.; Vilesov, A. F. Fast Nuclear Spin Conversion in Water Clusters and Ices: A Matrix Isolation Study. *J. Phys. Chem. A* **2011**, *115*, 9682−9688.

(12) Turgeon, P.-A.; Ayotte, P.; Lisitsin, E.; Meir, Y.; Kravchuk, T.; Alexandrowicz, G. Preparation, Isolation, Storage, and Spectroscopic Characterization of Water Vapor Enriched in the *ortho*-H_2O Nuclear Spin Isomer. *Phys. Rev. A: At., Mol., Opt. Phys.* **2012**, *86*, 062710.

(13) Turgeon, P.-A.; Vermette, J.; Alexandrowicz, G.; Peperstraete, Y.; Philippe, L.; Bertin, M.; Fillion, J.-H.; Michaut, X.; Ayotte, P. Confinement Effects on the Nuclear Spin Isomer Conversion of H_2O. *J. Phys. Chem. A* **2017**, *121*, 1571−1577.

(14) Bunker, Ph.; Jensen, P. In *Frontiers of Molecular Spectroscopy*; Laane, Jaan, Ed.; Elsevier, 2008; p 331.

(15) Votava, O.; Horká-Zelenková, V.; Rakovský, J.; Svoboda, V.; Fárnik, M. H_2O Nuclear-Spin Conservation/Relaxation in Supersonic Jet Expansion Probed by Quantitative Direct Absorption Spectroscopic Detection. *The 23-rd International Conference on High Resolution Molecular Spectroscopy*, September 2−6, 2014, Bologna, p 134.

(16) Konyukhov, V. K.; Prokhorov, A. M.; Tikhonov, V. I.; Faizulaev, V. N. Rotationally Selective Condensation of Heavy Water in a Supersonic Carbon Dioxide Jet. *JETP Lett.* **1986**, *43*, 85.

(17) Cirtog, M.; Asselin, P.; Soulard, P.; Tremblay, B.; Madebène, B.; Alikhani, M. E.; Georges, R.; Moudens, A.; Goubet, M.; Huet, T. R.; et al. The $(CH_2)_2O$-H_2O Hydrogen Bonded Dimer. *Ab initio* Calculations and FTIR Spectroscopy from Neon Matrix, and a New Supersonic Jet Experiment Coupled to the Infrared AILES Beamline of Synchrotron SOLEIL. *J. Phys. Chem. A* **2011**, *115*, 2523−2532.

(18) Häber, T.; Schmitt, U.; Emmeluth, C.; Suhm, M. A. Ragout-jet FTIR Spectroscopy of Cluster Isomerism and Cluster Dynamics: from Carboxylic Acid Dimers to N_2O Banoparticles. *Faraday Discuss.* **2001**, *118*, 331−359.

(19) Zischang, J.; Suhm, M. A. Infrared Absorption Imaging of 2D Supersonic Jet Expansions: Free Expansion, Cluster Formation, and Shock Wave Patterns. *J. Chem. Phys.* **2013**, *139*, 024201.

(20) Moudens, A.; Georges, R.; Goubet, M.; Makarewicz, J.; Lokshtanov, S. E.; Vigasin, A. A. Direct Absorption Spectroscopy of Water Clusters Formed in a Continuous Slit Nozzle Expansion. *J. Chem. Phys.* **2009**, *131*, 204312.

(21) Chehrouri, M.; Fillion, J.-H.; Chaabouni, H.; Mokrane, H.; Congiu, E.; Dulieu, F.; Matar, E.; Michaut, X.; Lemaire, J. L. Nuclear Spin Conversion of Molecular Hydrogen on Amorphous Solid Water in the presence of O_2 traces. *Phys. Chem. Chem. Phys.* **2011**, *13*, 2172−2178.

(22) Redington, R. L.; Milligan, D. E. Molecular Rotation and *ortho*−*para* Nuclear Spin Conversion of Water Suspended in Solid Ar, Kr, and Xe. *J. Chem. Phys.* **1963**, *39*, 1276.

(23) Georges, R.; Bonnamy, A.; Benidar, A.; Decroi, M.; Boissoles, J. FTIR Free-Jet Set-up for the High Resolution Spectroscopic Investigation of Condensable Species. *Mol. Phys.* **2002**, *100*, 1551−1558.

(24) Miller, D. R. In *Atomic and Molecular Beam Methods*; Scoles, G., Ed.; Oxford University Press: New York, 1988; Vol. *1*.

(25) Pauly, H. *Atom, Molecule, and Cluster Beams I: Theory, Production and Detection of Thermal Energy Beams*; Springer-Verlag: Berlin, Heidelberg, Germany, 2000.

(26) Bonnamy, A.; Georges, R.; Benidar, A.; Boissoles, J.; Canosa, A.; Rowe, B. R. Infrared Spectroscopy of $(CO_2)_N$ Nanoparticles ($30< N <$ 14500) Flowing in a Uniform Supersonic Expansion. *J. Chem. Phys.* **2003**, *118*, 3612−3621.

(27) Belikov, A. E.; Sharafutdinov, R. G. Rotational Relaxation Time in Free Jets of He + N_2 Mixtures. *Chem. Phys. Lett.* **1995**, *241*, 209−214.

(28) Herman, M.; Georges, R.; Hepp, M.; Hurtmans, D. High resolution Fourier transform spectroscopy of jet-cooled molecules. *Int. Rev. Phys. Chem.* **2000**, *19*, 277−325.

(29) *Handbook of High Resolution Spectroscopy*; Quack, M., Merkt, F., Ed.; John Wiley and Sons, 2011; Vol. *II*, pp 970−977.

(30) Mandin, J.-Y.; Flaud, J.-M.; Camy-Peyret, C.; Guelachvili, G. Measurements and Calculations of Self-Broadening Coefficients of

DOI: 10.1021/acs.jpca.7b06858
J. Phys. Chem. A XXXX, XXX, XXX−XXX

Lines Belonging to the ν_2 Band of $H_2{}^{16}O$. *J. Quant. Spectrosc. Radiat. Transfer* **1980**, *23*, 351−370.
(31) *PAC, Glossary of Terms Used in Photochemistry (IUPAC Recommendations 1996)*; 1996; Vol. *68*, p 2223. DOI: 10.1351/pac199668122223.
(32) Rothman, L. S.; Jacquemart, D.; Barbe, A.; Chris Benner, D.; Birk, M.; Brown, L. R.; Carleer, M. R.; Chackerian, Jr.; Chance, K.; Coudert, L. H.; et al. The HITRAN 2004 Molecular Spectroscopic Database. *J. Quant. Spectrosc. Radiat. Transfer* **2005**, *96*, 139−204.
(33) Simeckova, M.; Jacquemart, D.; Rothman, L. S.; Gamache, R. R.; Goldman, A. Einstein A-Coefficients and Statistical Weights for Molecular Absorption Transitions in the HITRAN Database. *J. Quant. Spectrosc. Radiat. Transfer* **2006**, *98*, 130−155.
(34) Votava, O.; Masat, M.; Pracna, P.; Kassi, S.; Campargue, A. Accurate Determination of Low State Rotational Quantum Numbers (J < 4) from Planar-Jet and Liquid Nitrogen Cell Absorption Spectra of Methane Near 1.4 micron. *Phys. Chem. Chem. Phys.* **2010**, *12*, 3145−3155.
(35) Bourgalais, J.; Roussel, V.; Capron, M.; Benidar, A.; Jasper, A. W.; Klippenstein, S. J.; Biennier, L.; Le Picard, S. D. Low Temperature Kinetics of the First Steps of Water Cluster Formation. *Phys. Rev. Lett.* **2016**, *116*, 113401.

DOI: 10.1021/acs.jpca.7b06858
J. Phys. Chem. A XXXX, XXX, XXX−XXX